The cross-correlation search for a hot spot of gravitational waves : Numerical study for point spread function

The cross-correlation search for a hot spot of gravitational waves : Numerical study for point spread function

Yuta Okada[1], Nobuyuki Kanda[1*], Sanjeev Dhurandhar[2], Hideyuki Tagoshi[3] and Hirotaka Takahashi[4,5]

[1] Graduate School of Science, Osaka City University, Sumiyoshi-ku, Osaka 558-8585, Japan
[2] Inter-University Centre for Astronomy and Astrophysics, Post Bag 4, Ganeshkhind, Pune 411007, India
[3] Department of Earth and Space Science, Graduate School of Science, Osaka University, Toyonaka, Osaka 560-0043, Japan
[4] Department of Humanities, Yamanashi Eiwa College, 888, Yokone, Kofu, Yamanashi 400-8555, Japan
[5] Earthquake Research Institute, University of Tokyo, Bunkyo-Ku, Tokyo 113-0032, Japan
[*] Paper presented at the conference by N. Kanda

E-mail: kanda@sci.osaka-cu.ac.jp

Abstract. The cross-correlation search for gravitational waves, also known as 'radiometry', has been previously applied to map the gravitational wave stochastic background in the sky and also to target gravitational waves from rotating neutron stars/pulsars. We consider the Virgo cluster which may appear as a 'hot spot' spanning few pixels in the sky in a radiometry analysis. Our results show that sufficient signal to noise ratio can be accumulated with integration times of the order of a year. We also present a numerical simulation of radiometric analysis, assuming ground-based detectors which are currently under construction or being upgraded. The point spread function of the injected sources is confirmed by numerical tests. The typical resolution of radiometry analysis is a few square degrees, as compared to the several thousand pixels for the full sky in an all-sky map.

1. Introduction

Ground-based gravitational wave detectors currently being constructed or upgraded may reach the strain sensitivity of the order of $10^{-24}[1/\sqrt{\mathrm{Hz}}]$ in the near future. The detector sites are widely distributed around the globe, which makes independent observation of gravitational waves possible. Since the distributed detectors may not have correlated noise but will have a correlation in the gravitational signal, the cross-correlation of data from two or more detectors makes is a possible way to search for unknown gravitational waveforms. This is a useful property for gravitational wave searches esecially for short duration bursts, or for long duration stochastic gravitational waves. The measurements from spatially separated detectors allow triangulation of the source. The time delay between detectors can be used to determine the incident direction of the gravitational wave in short duration signal analysis. On the other hand, employment of the time delay term in searches for long duration signals or stochastic gravitational waves which come from an arbitrary direction is not simple.

However, we can extract the signal strength if we deconvolve the Earth's rotation from the signal for any point in the sky. Using multiple detectors and long integration times, the deconvolution is possible. This type of directional cross-correlation search for gravitational waves is known as 'radiometry'.

Radiometry and any other triangulation analysis requires widely separated detectors - long baselines, and the variation of orientation (zenith direction, and azimuthal rotation of interferometers) to cover the sky and resolve the polarizations. The recent beginning of the construction of LCGT[1] in addition to previously constructed advanced detector sites of LIGO[2] and Virgo[3] encourage the development of radiometric analysis.

1.1. Radiometry Filter

Gravitational wave radiometry is a type of stochastic gravitational wave search, but it is also directed or targeted. Radiometric analysis assumes that gravitational waves come from a particular direction such as a point like source or a 'hot spot' in the sky. The radiometry filter uses data from at least two detectors and does not require the knowledge of the waveform. Gravitational waves coming from a particular direction will have a time of arrival delay at two detectors as shown in Fig.1. Since gravitational wave signals at both detectors are coherent in the same polarization component, we can extract gravitational wave signals in the cross-correlation product from two detectors observations with appropriate time delay. Moreover, the signal-to-noise ratio for the gravitational wave will be increased with long integration time, because the two detector noises are independent. By changing the source direction sequentially after every step, we can construct a gravitational wave 'sky map' by radiometric analysis.

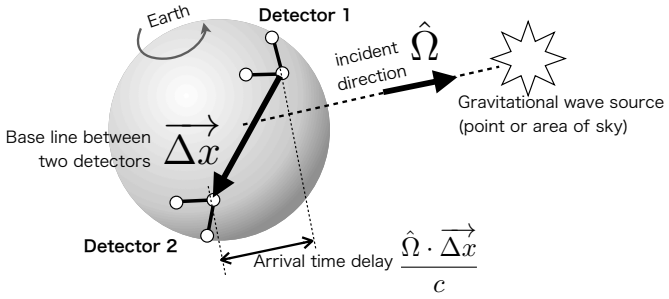

Figure 1. Ideal setup of a radiometry analysis.

Radiometry analysis has been proposed and studied in previous works[4][5]. We explain the radiometry filter briefly here. The source direction or trial direction of the search can be represented by a unit vector $\hat{\Omega}$. The two detectors are labelled as 1 and 2, and the base-line from detector 1 to detector 2 is denoted by the vector $\overrightarrow{\Delta x}$. The arrival time delay for the gravitational wave between the two detectors is $\frac{\hat{\Omega}\cdot\overrightarrow{\Delta x}}{c}$, where c is the speed of light. The output from each detector $s_1(t), s_2(t - \frac{\hat{\Omega}\cdot\overrightarrow{\Delta x}}{c})$ in the time domain has the same gravitational wave timing. In the Fourier domain, this time delay represents a phase difference of the detectors output $\tilde{s}_1(f), \tilde{s}_2(f)$, the Fourier transform of $s_1(t)$ and $s_2(t)$. Therefore, we can define the radiometry filter as follows. A directed overlap reduction function $\gamma(f, \hat{\Omega})$ can be defined to correct the phase difference as

$$\gamma(f, \hat{\Omega}) = \sum_{A=+,\times} F_1^A F_2^A e^{i2\pi f \frac{\hat{\Omega}\cdot\overrightarrow{\Delta x}}{c}} \ , \tag{1}$$

where $F^A_{1,2}$ are the antenna pattern[6] of detector 1 or 2 for each polarization $A = +$ or $\times$ of the gravitational wave. For optimal filtering, we employ the detectors noise power spectrum $P_{1,2}(f)$ respectively, and assume that gravitational wave spectrum is $H(f)$. The radiometry filter can defined as

$$Q(f,\hat{\Omega}) = \lambda \frac{\gamma^*(f,\hat{\Omega})H(f)}{P_1(f)P_2(f)} \ , \tag{2}$$

and the filter output is

$$\Delta S(\hat{\Omega}) = \int_{-\infty}^{\infty} df \ \tilde{s}_1^*(f)\tilde{s}_2(f)Q(f,\hat{\Omega}). \tag{3}$$

The base-line $\overrightarrow{\Delta x}$ will change in celestial coordinates according to Earth's rotation in the case of ground-based detectors. Therefore, we calculate ΔS over a short time slice ('chunk') $t - \Delta t/2$ and $t + \Delta t/2$. Therefore the quantities defined in the above equations also become functions of t. Thus the Fourier transforms of detector data can be represented using the short Fourier transforms of $\tilde{s}^*_{1,2}(t;f)$, and $Q(f)$ becomes $Q(t,f)$ and so on. Then

$$\Delta S(t,\hat{\Omega}) = \int_{-\infty}^{\infty} df \ \tilde{s}_1^*(t;f)\tilde{s}_2(t;f)Q(t,f,\hat{\Omega}). \tag{4}$$

Processing many chunks for long duration observational data, we can determine the statistics of ΔS. Since the gravitational wave component will appear in the real part of ΔS, we employ the mean $\mu(\hat{\Omega})$

$$\mu_{\Delta S}(\hat{\Omega}) = \langle \Re[\Delta S] \rangle \ , \tag{5}$$

and the standard deviation $\sigma_{\Delta S}(\hat{\Omega})$ for the real part of ΔS.

We now need to sum up over the contributions to the SNR, which we denote by $\rho(\hat{\Omega})$, for all the chunks making up the total observation period. The statistic for the full observation time is denoted by $S(\hat{\Omega})$ and its mean and standard deviation by $\mu(\hat{\Omega})$ and $\sigma(\hat{\Omega})$ respectively. The signal-to-noise ratio of particular direction $\hat{\Omega}$ is then given by:

$$\rho(\hat{\Omega}) = \mu(\hat{\Omega})/\sigma(\hat{\Omega}). \tag{6}$$

2. Hot Spot of Gravitational Wave Radiometry

A radiometry analysis might find a hot spot in the sky map. A hot spot may be formed by a concentration of a large number of unresolved astronomical sources. One of the promising targets is the Virgo cluster, which could contain $\sim 10^{11}$ neutron stars. Our results show that sufficient signal to noise can be accumulated with integration times of the order of a year. We published this study in the reference [7]. If the average ellipticity of neutron stars is 10^{-6}, Virgo cluster might appear as a hot spot with observation of order of year, using 2nd generation ground-based detectors. The numerical estimation of the expected GW spectrum and signal-to-noise ratio of a Virgo cluster hot spot is explained in this reference in detail.

Here we remark on the average detector response as a function of source declination. In eq.(1), the magnitude of two detector's combined detector response $\Gamma(\hat{\Omega},t)$ is given as

$$\Gamma(\hat{\Omega},t) = F_{+1}(\hat{\Omega},t)F_{+2}(\hat{\Omega},t) + F_{\times 1}(\hat{\Omega},t)F_{\times 2}(\hat{\Omega},t). \tag{7}$$

Since $\Gamma(\hat{\Omega},t)$ will change according to Earth's rotation, we wish to use the average over day:

$$\langle \Gamma^2 \rangle_{1\mathrm{day}}(\hat{\Omega}) = \frac{1}{T_{1\mathrm{day}}} \int_0^{1\mathrm{day}} \Gamma^2(\hat{\Omega},t)\, dt. \tag{8}$$

$\langle \Gamma^2 \rangle$ will not depend on the right ascension. Fig.2 displays the square root of $\langle \Gamma^2 \rangle$. For the Virgo cluster whose center is at declination of about $12°4'59''$, LCGT and the India site (IndIGO[8]) is a good combination. Using several detector combinations will cover the whole sky in radiometry analysis.

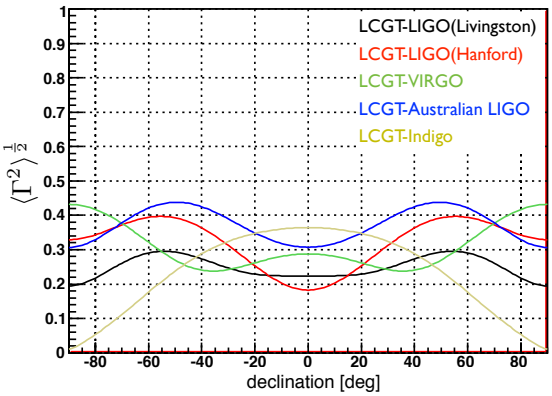

Figure 2. Average of detector response Γ^2 as a function of celestial declination angle.

3. Numerical Simulation: Source Injection Test

To confirm the behavior of a hot spot in the radiometry sky map, we construct a numerical test of the radiometry filter. It consists of the following steps.

1) segment the data stream into short duration *'chunks'* : In real observational data processing, steps 2) 5) are performed time series data split into short duration 'chunks'.

2) generate gravitational wave detector noise: Assuming the design noise spectrum [9] [10] [11] [12] of each detector and injecting random gaussian noise, we generate time series of noise $n(t)$. In this paper, the data sampling frequency is 4000 Hz, and the chunk length is 65.536 sec. In the study of the point spread function in next subsection, we skip noise generation and use the gravitational wave signal only.

3) generate gravitational wave signal: The gravitational wave signal at the source is generated. We test with a sinusoidal wave, and random phase waveform which has a flat power spectrum in a certain frequency band, e.g. flat power spectrum in 300±30 Hz.

4) inject gravitational wave signal into detector noise in the time domain: The gravitational wave signal in the detectors will be affected by the Doppler effect, antenna patterns and time delay between the detectors. The Doppler effect is appears as a frequency modulation of the gravitational wave in the detector according to the orbital and rotational motion of the Earth. The antenna patterns $F_+, F_\times$ are calculated for the incident direction. Also the arrival time difference of the signal on two (or more) detectors are given in this step. These quantities will change as a function of time due to the Earth's motion.

5) calculate radiometry filter output $\Delta S(t, \hat{\Omega})$: We calculate radiometry filter output of this chunk in eq.(4) using two detectors for the particular direction $\hat{\Omega}$ of a *'pixel'*. Changing $\hat{\Omega}$ step by step, sweeping over all the sky, we calculate $\Delta S(t, \hat{\Omega})$ for all pixels.

6) repeat step 1) – 5) for next chunk: We iterate steps above for all chunks.

Finally,

7) sum up ΔS and calculate the signal-to-noise ratio $\rho(\hat{\Omega})$ of each pixel: We sum up each chunk's output $\Delta S(t, \hat{\Omega})$ with respect to each pixel. Then we get $\mu(\hat{\Omega}), \sigma(\hat{\Omega})$ and calculate the signal-to-noise ratio $\rho(\hat{\Omega})$ in eq.(6). The $\rho(\hat{\Omega})$ are displayed as pixels of a sky map with color according to its magnitude as in Fig.3.

Fig.4 displays a schematic data flow of our numerical test of the radiometry filter. We tried various combinations of current detectors, and Fig.4 displays LCGT and advanced LIGO as an example. For studying the point spread behavior in the following sections of this paper, we use the case of LCGT and advanced LIGO at Livingston.

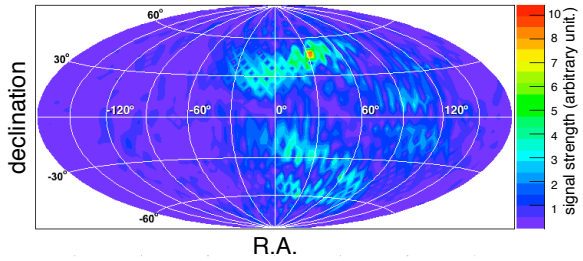

Figure 3. Example radiometry sky map. This map is displayed in celestial coordinates. Red small area (R.A. 30 degree, declination 45 degree) is corresponding to the injected gravitational wave source.

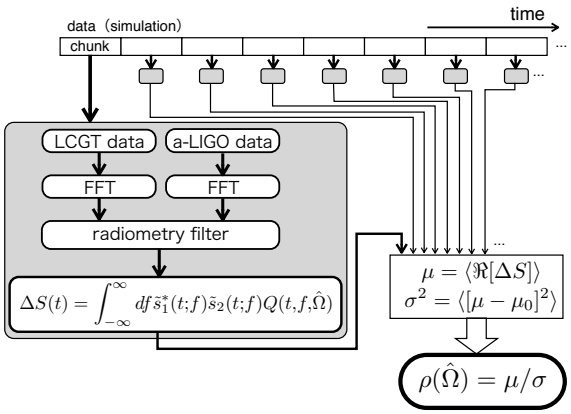

Figure 4. Data flow of numerical test of the radiometry filter.

3.1. Point Spread Function

How spread out a point source appears on the sky is important for evaluating the feasibility of searches. This is called the *'point spread function'*. The point spread function depends on the gravitational wave frequency or spectrum, the position on the sky (right ascension, celestial declination), and on the detector orientation on the Earth. In the point spread function study in this subsection, we used noiseless detector output, but the other filter settings are the same as above. Thus, the magnitude of the gravitational wave in this section is arbitrary. Our test gravitational wave signal has a flat spectrum around f_0 [Hz] given by

$$H(f) = \begin{cases} 1 & (0.9f_0 \leq f \leq 1.1f_0) \\ 0 & (\text{otherwise}). \end{cases} \tag{9}$$

The injected signal for each chunk fluctuates as a stochastic signal whose phase is random.

Fig.5 shows the point spreading for some frequency samples in a single chunk process. In a single chunk, we can find wide and multiple spreading images from the injection of a point source. These multiple images occur for sky positions where the time delay along the two-detector baseline differs from the correct delay by an integer number of periods of the central frequency of the narrowband signal. The spatial interval is wide for low frequency band width, and narrow for higher frequency bandwidth. But in general, it is hard to identify the exact position of the point source in a single chunk map, even if the gravitational wave is strong.

As the Earth rotates, the multiple (aliased) images will change position as the detector orientation relative to the source changes. Therefore, during a long integration time, aliases will be reduced and the true signal position will build up with stacking filter output coherently. Fig.6 displays a radiometry map with one day integration for a narrow region around the

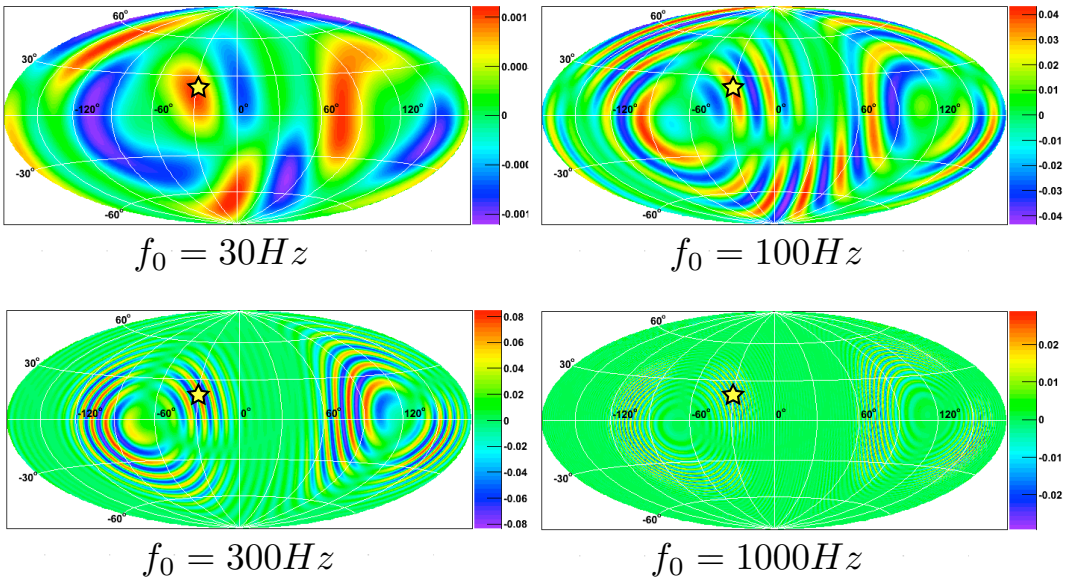

Figure 5. Radiometry filter output of a single chunk with various frequency signals with the LCGT and LIGO Livingston. The star symbol shows the true injection position. The gravitational wave has a flat spectrum around f_0 [Hz] with $\pm$ 10% of f_0 [Hz] width; e.g. f_0=300Hz means from 270Hz to 330Hz. The chunk duration is 65.536 sec.

injection sources. The figure displays variation in declination angle of $\delta = 15°, 45°$and $75°$. The point spread function is not dependent on right ascension with more than one day integration. According to the combined detector response as eq.(7) and eq.(8) with the LCGT and LIGO Livingston, mid declination angles have a circular image spread. On the other hand, in low and high declination areas, the point spread function is an ellipsoid.

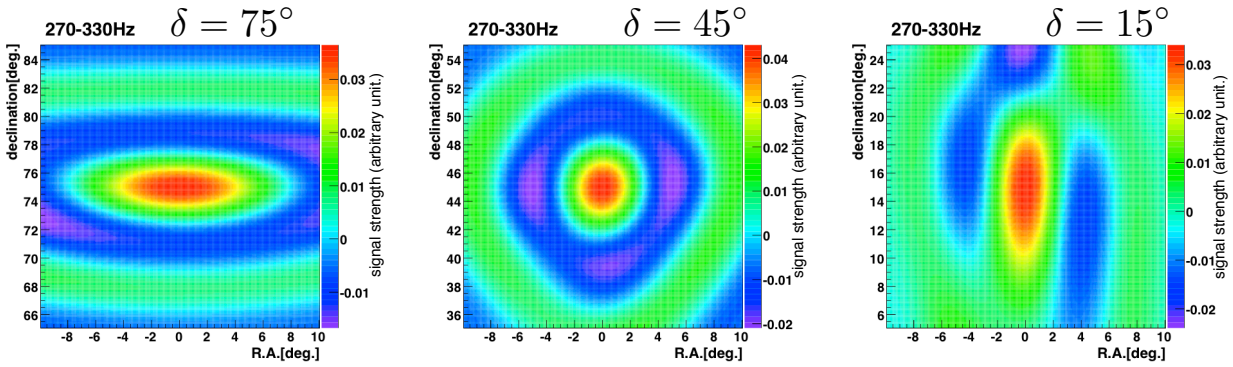

Figure 6. Point spread image in radiometry map (zoomed in) with one day integration for various declination angles with the LCGT and LIGO Livingston. The frequency f_0 of the injected signal is 300 Hz. The declination angles are $\delta = 15°, 45°$and $75°$ respectively.

The spread of a point source is strongly dependent on the gravitational wave frequency. Its order is determined by the diffraction limit $\frac{\lambda}{|\overrightarrow{\Delta x}|}$, where λ is the wave length of the gravitational

wave and the distance between the detectors is $|\overrightarrow{\Delta x}|$. Fig.7 displays some examples of the image spread for a point injection at $\delta = 60°$. The signal at 30 Hz spreads widely. The 1kHz signal has aliases as concentric circles, but the true injected point appears as in intense peak.

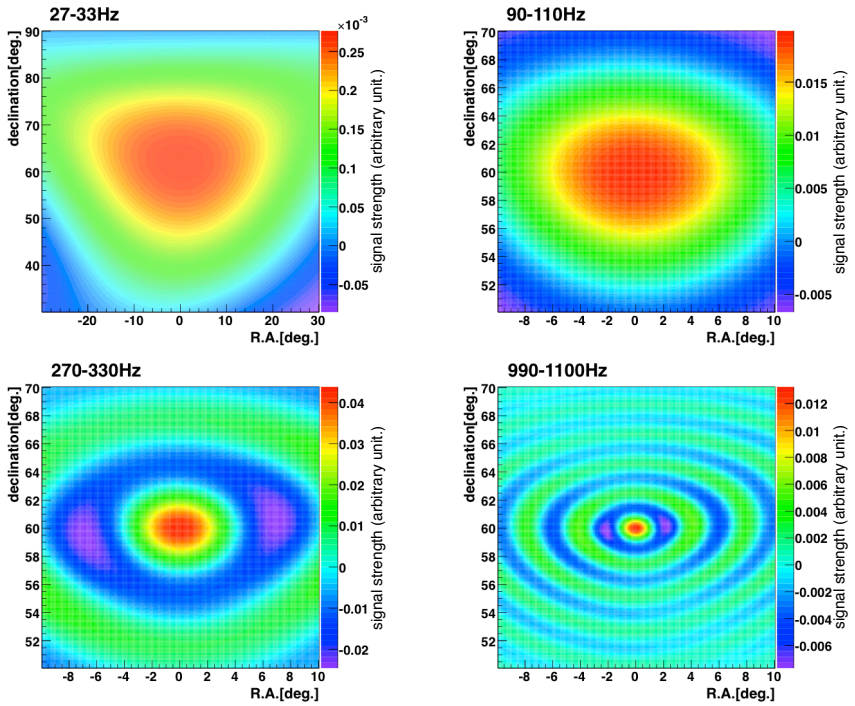

Figure 7. Point spread image in a radiometry map with one day integration for variation of gravitational wave frequencies with the LCGT and LIGO Livingston. The injection point is at $\delta = 60°$. The central frequency of each figure is 30Hz, 100Hz, 300Hz and 1kHz respectively.

To qualify this spreading, we define the spread size as the solid angle $\Delta\Omega$ [sr] of the area which is larger than half the height of the local peak. Fig.8 displays the relation between $\Delta\Omega$ and the frequency of the gravitational wave. The solid line is $\dfrac{\lambda}{|\overrightarrow{\Delta x}|}$ and the dashed line is an empirical approximation for the high δ region :

$$\sim \pi \left(\frac{1}{2} \frac{c}{f\ |\overrightarrow{\Delta x}|} \right)^2 \times \left(\frac{80 - \delta\ [\mathrm{deg.}]}{100} \right) [\mathrm{sr}]. \tag{10}$$

In the Fig.8, we also display the corresponding apparent diameter for the y-axis in the case of a circular image.

3.2. Optimal Pixel Size

Point spreading suggests an optimal size of pixels. It is possible to employ pixels of a similar size to the point spread function, because this is the angular resolution of the radiometry analysis. However, there is no need to divide the celestial sphere finely that one pixel is far smaller than the point spread function. Fig.9 displays the optimal number of pixels in the sky when we use the as point spread size (solid angle) as the pixel size. In this study with the LCGT and LIGO Livingston base line can employ up to several thousand pixels for the good sensitivity frequency band of the detectors, around $100 \sim 300$ Hz.

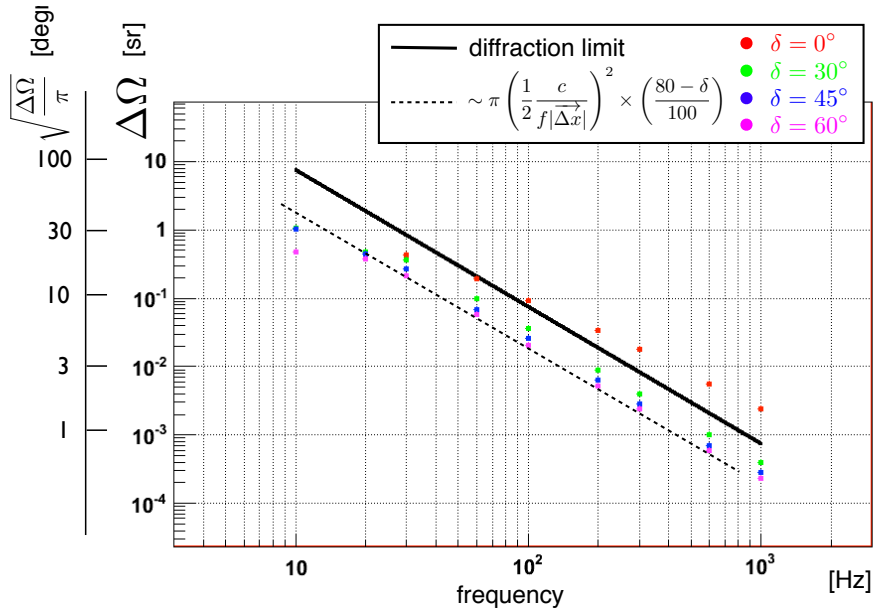

Figure 8. Point spread size of injected gravitational waves. Points are injected gravitational wave signals with different central frequency f_0 and variation of declination angle δ. The x-axis is the gravitational wave frequency, and the y-axis is the solid angle of point spreading. The y-axis also displays the corresponding apparent diameter for the case of a circular image.

The Earth rotation during one chunk length ($\sim$ 65 sec.) in this analysis is approximately 0.25 degree. This is closer to the diffraction limit in high frequency bandwidth $\sim$ 1 KHz. Therefore, we have to use shorter chunks to get the fine resolution for high frequency bandwidth.

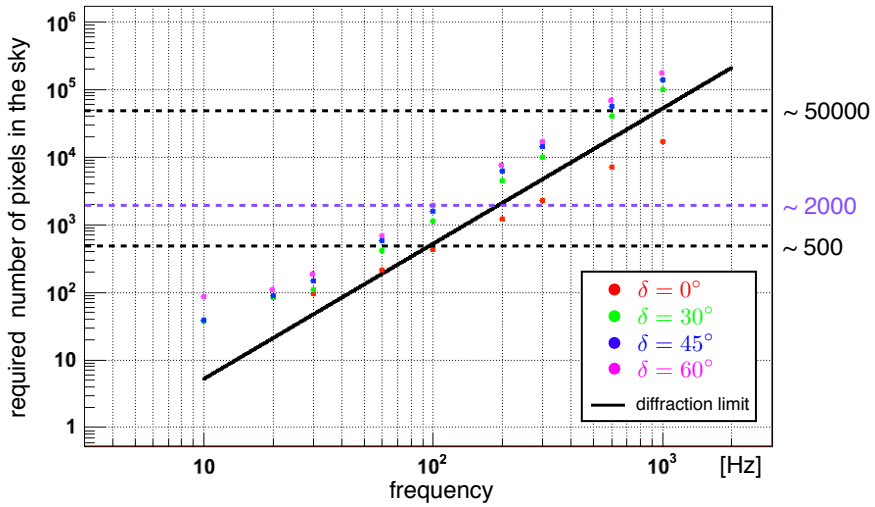

Figure 9. Optimal number of pixels to cover the sky when we use the as point spread size (solid angle) as the pixel size. The solid line corresponds to the diffraction limit size.

4. Summary

We have studied radiometry analysis for stochastic gravitational waves of astronomical origin, which might have an anisotropy or local excess. The Virgo cluster may appear as a 'hot spot' on the radiometry map of the sky with advanced and third generation gravitational wave detectors. We have performed numerical simulations with a radiometry filter, and displayed the image spread for point like gravitational wave sources, with the LCGT and advanced LIGO combination. Other combinations of the global network detectors will be useful to determine the signal properties. We are planning to proceed with injection tests for multiple sources and sources spread over areas larger than the point spread function.

Acknowledgments

S. Dhurandhar acknowledges the DST and JSPS Indo-Japan international cooperative programme for scientists and engineers for supporting visits to Osaka City University, Japan and Osaka University, Japan. H. Tagoshi, N. Kanda and H. Takahashi thank JSPS and DST under the same Indo-Japan programme for their visit to IUCAA, Pune, India. N.Kanda's work was supported in part by a Monbu Kagakusho Grant-in-aid for Scientific Research of Japan (No. 23540346). H.Tagoshi's work was also supported in part by a Monbu Kagakusho Grant-in-aid for Scientific Research of Japan (Nos. 20540271 and 23540309). H.Takahashi's work was also supported in part by a Monbu Kagakusho Grant-in-aid for Scientific Research of Japan (No. 23740207).

References

[1] K. Kuroda and the LCGT Collaboration, Classical Quantum Gravity 23, S215 (2006).
[2] B. P. Abbott et al., Rep. Prog. Phys. 72 (2009) 076901
[3] T. Accadia et al., Class. Quantum Grav. 28 114002
[4] S. Mitra, S. V. Dhurandhar, T. Souradeep, A. Lazzarini, V. Mandic, S. Bose, and S. Ballmer, Phys. Rev. D 77, 042002 (2008).
[5] D. Talukder, S. Mitra, and S. Bose, Phys. Rev. D 83, 063002 (2011).
[6] P. Jaranowski, A. Krolak, and B. F. Schutz, Phys. Rev. D 58, 063001 (1998).
[7] S. V. Dhurandhar, H. Tagoshi, Y. Okada, N. Kanda and H. Takahashi, Phys. Rev. D 84, 083007 (2011)
[8] http://www.gw-indigo.org/
[9] http://gwcenter.icrr.u-tokyo.ac.jp/researcher/parameters
[10] https://dcc.ligo.org/cgi-bin/DocDB/ShowDocument?docid=2974
[11] https://wwwcascina.virgo.infn.it/advirgo/
[12] http://www.et-gw.eu/etsensitivities